



Antibacterial activity and inflammation inhibition of ZnO nanoparticles embedded TiO₂ nanotubes

Shenglian Yao^{1,4} , Xujia Feng^{1,4}, Jiaju Lu², Yudong Zheng¹ ,
Xiumei Wang², Alex A Volinsky³ and Lu-Ning Wang¹

¹ State Key Laboratory for Advanced Metals and Materials, School of Materials Science and Engineering, University of Science and Technology Beijing, Beijing 100083, People's Republic of China

² School of Materials Science and Engineering, Tsinghua University, Beijing 100084, People's Republic of China

³ Department of Mechanical Engineering, University of South Florida, 4202 E. Fowler Ave. ENB118, Tampa, FL 33620, United States of America

E-mail: luning.wang@ustb.edu.cn

Received 16 January 2018, revised 22 March 2018

Accepted for publication 29 March 2018

Published 16 April 2018



CrossMark

Abstract

Titanium (Ti) with nanoscale structure on the surface exhibits excellent biocompatibility and bone integration. Once implanted, the surgical implantation may lead to bacterial infection and inflammatory reaction, which cause the implant failure. In this work, irregular and nanorod-shaped ZnO nanoparticles were doped into TiO₂ nanotubes (TNTs) with inner diameter of about 50 nm by electro-deposition. The antibacterial properties of ZnO incorporated into TiO₂ nanotubes (TNTs/ZnO) were evaluated using *Staphylococcus aureus* (*S. aureus*). Zn ions released from the nanoparticles and the morphology could work together, improving antibacterial effectiveness up to 99.3% compared with the TNTs. Macrophages were cultured on the samples to determine their respective anti-inflammatory properties. The proliferation and viability of macrophages were evaluated by the CCK-8 method and Live&Dead stain, and the morphology of the cells was observed by scanning electron microscopy. Results indicated that TNTs/ZnO has a significant inhibitory effect on the proliferation and adhesion of macrophages, which could be used to prevent chronic inflammation and control the inflammatory reaction. Besides, the release of Zn ions from the ZnO nanoparticles is a long-term process, which could be beneficial for bone integration. Results demonstrate that ZnO deposited into TNTs improved the antibacterial effectiveness and weakened the inflammatory reaction of titanium-based implants, which is a promising approach to enhance their bioactivity.

Keywords: TiO₂ nanotubes, ZnO nanoparticles, bacterial inhibition, immune inhibition

(Some figures may appear in colour only in the online journal)

1. Introduction

Titanium and its alloys are widely used for orthodontic and orthopedic implants because of their excellent biocompatibility and mechanical properties [1, 2]. Early bone formation and osseointegration are essential for the implantation success. To achieve appropriate tissue acceptance and rapid bone

formation during and after implantation, surface modification is crucial for interaction between the implant and the surrounding tissue. During the last decade, several surface modification approaches have been reported to improve the bioactivity on Ti implants [3, 4]. Current research is becoming increasingly focused on fabrication of anodic TiO₂ nanopores/nanotubes, which simulate the size and the arrangement of collagen fibrils in bone tissues [5]. Additionally, nanostructures are characterized by a high aspect

⁴ These authors contributed equally.

Table 1. Elemental content of TNTs/ZnO.

Sample	Electrolyte concentration mM	Time min	EDS atomic ratio			ICP ppm, total Zn
			Ti	O	Zn	
TNTs/ZnO-1	5	5	44.05	53.86	2.09	1.7
TNTs/ZnO-2	5	20	43.35	54.19	2.46	3.4
TNTs/ZnO-3	1	100	38.19	56.27	5.54	5.8

ratio, proving abundant sites for cells to adhere and proliferate. Several groups have shown that TiO₂ nanotubes promoted the spread, proliferation and migration of bovine epithelial cells and the proliferation of osteoblasts *in vitro* [6]. Detailed research on TiO₂ nanotubes with different diameters showed that small diameter (<30 nm) is conducive to human mesenchymal stem cells (MSCs) proliferation and adhesion, while the large size (>70 nm) may promote osteoblastic differentiation [7, 8].

However, similar to osteoblast cells and MSCs, nanotubular structures can also accelerate bacterial adhesion. Bacterial infections, such as *Staphylococcus aureus* (*S. aureus*) and *Escherichia coli*, always resulted in blocking bone formation and leading to implant failure. It was shown that *S. aureus* increased adhesion and proliferation along with MSCs [9]. Thus, improving antibacterial properties of nanotubular structures is crucial. Various antibacterial agents were incorporated into nanotubes to achieve bacterial inhibition [10–12]. For example, antibiotic [13–15], antibacterial peptides [16] and metallic elements, including Ag [17–19], Zn [18–22] and Se [23, 24] were embedded to enhance the antibacterial properties. Among those antibacterial pharmaceutical agents, Zn, especially ZnO nanoparticles have shown excellent capability of inhibiting *S. aureus in vitro* and *in vivo* [20, 25].

Another consideration is that success of metallic implants is often limited by macrophage-related inflammation [26]. Cytokines, chemokines and growth factors caused by macrophages could affect the progress of inflammation and healing [27]. For example, the secretion of tumor necrosis factor- α by macrophages could regulate the surrounding cells and control wound healing [28]. Thus, it is important to find an effective way to suppress immune response in limiting inflammation and preventing implant failure. It was found that the size of nanotubular arrays had significant effect on the behavior of macrophages. It was also reported that ZnO could influence proliferation, viability and migration of macrophages to retard immune response [29–31]. Additionally, Zn is an important trace element in the human body and can improve DNA synthesis, enzyme activity, and nucleic acid metabolic activity [32]. Zn ions have the ability to promote osteoblast proliferation and enhance biomineralization [33, 34].

Herein, to achieve bacterial and inflammatory inhibition on the TiO₂ nanotubular surface, two types of ZnO nanoparticles (irregular shaped and nanorod-type) were incorporated into TiO₂ nanotubes by electrodeposition with

optimizing chemical concentration in electrolytes and the reaction time. *S. aureus* proliferation and viability were used to evaluate the antibacterial properties. RAW 264.7 cells were cultured on TNTs and ZnO incorporated TiO₂ nanotubes (TNTs/ZnO) to determine immune inhibition.

2. Materials and methods

2.1. Sample preparation and characterization

2.1.1. Fabrication of TNTs. TiO₂ nanotubular arrays (TNTs) were fabricated by anodization as in previous work [35]. Pure Ti discs (>99.7% pure, Φ 14.5 mm \times 1 mm) were mechanically polished with different abrasive papers (from 600 to 2000 grit). All the samples were sonicated in acetone, ethanol and deionized water for 15 min, respectively. Before the anodization, all discs were acid-etched in a mixture solution (volume ratio of HF:HNO₃:H₂O is 1:4:2) for 3 s, then washed with deionized water and dried in air. A two-electrode configuration was used for the anodization. The Ti discs were used as the anode, and Pt foil was the cathode. The nanotubular arrays on the Ti surface were fabricated in ethylene glycol with 2 vol% H₂O and 2.5 g l⁻¹ NH₄F at 40 V. In order to strictly control the diameter of nanotubes, two-step anodization approach was selected. In the first step, the samples were anodized at 40 V for 2 h. After the first-step anodization, the oxide layer on the surface of Ti sheets were removed by treating with a reverse voltage of 4 V in 0.5 M H₂SO₄ and sonicated in distilled water. Subsequently, the samples were anodized for the second step through the same electrolyte and voltage as the first one for 1 h.

2.1.2. Fabrication of TNTs/ZnO. ZnO nanoparticles were incorporated into the TNTs by electrodeposition similar to the previous work [36]. The electrodeposition was carried out in a three-electrode configuration. The TNTs served as the working electrode. A saturated calomel electrode (SCE) and a Pt foil served as the reference and the counter electrodes, respectively. Two different concentrations of Zn(NO₃)₂ electrolyte bath solution (5 mM and 1 mM) were used to fabricate ZnO with a potential of $-0.9 V_{SCE}$ at 65 °C. As shown in table 1, samples were named TNTs/ZnO-1, TNTs-ZnO-2 and TNTs/ZnO-3, according to the differences in experimental conditions. Prior to cell and bacterial studies, all

the samples were annealed at 450 °C for 1 h in air with 1 °C min⁻¹ heating rate.

2.1.3. Characterization of TNTs/ZnO. The surface and cross-sectional morphology of TNTs and ZnO-incorporated TNTs was observed using field-emission scanning electron microscopy (FEI Nava450). All the samples were sputter-coated with a layer of nanoscale Au before observations. The samples were further characterized by making cross-sections and analyzing them by transmission electron microscopy (TEM, FEIF20). Elemental analysis was carried out using energy dispersive spectra (EDS, FEI Nava450) detector attached to the TEM. The total Zn element concentration was also determined by ICP-AES after the samples were dissolved in 1% HF and 1.5% HNO₃. In order to detect the presence of Zn element, x-ray photoelectron spectroscopy (XPS, Al target, PHI Quantera SXM) was used to determine the bonding states of the surface constituents.

2.1.4. Zn ion release. To monitor the amount of released Zn ions, all the samples were immersed in 40 ml phosphate-buffered saline (PBS) for 14 d. The concentration of Zn ions was measured by inductively coupled plasma atomic emission spectrometry (ICP-AES, MKIIM6) at different time points (2, 4, 6, 8 and 14 d).

2.2. Bacterial assays

2.2.1. Antibacterial test. Antibacterial capability of the TNTs/ZnO specimens was evaluated by examining the number of *S. aureus* (MRSA252; ATCC) during culturing. TNTs was selected as the control. Lysogeny broth (LB) medium was used to culture the bacteria. To access the antibacterial properties of released Zn ions in the supernatant, the bacteria with a density of 10⁴ CFU ml⁻¹ were seeded on all samples and then cultured at 37 °C for 24 h. The amount of surviving microorganisms was measured by ultraviolet spectrophotometer at a wavelength of 300 nm after dilution 10-folded steps with LB medium.

To determine the adhesion of bacteria on the tested materials, each sample was also incubated in 1 ml of the *S. aureus* at a concentration of 10⁴ CFU ml⁻¹. After 24 h culturing, the samples were gently rinsed with PBS three times to remove the non-adhered bacteria. The adhered *S. aureus* on each sample were detached into 5 ml of PBS by ultrasonic vibration for 5 min, and were diluted 1000-fold with PBS. Then, 100 μl of the diluted *S. aureus* suspension was inoculated onto TSA agar plates. After incubation for 24 h at 37 °C, bacterial colonies were counted by eye observation. The antibacterial effectiveness for the adhered *S. aureus* in the medium was calculated based on the following formula:

$$\text{Antibacterial effectiveness\%} = (A - B) / A \times 100\%, \quad (1)$$

where *B* represents the bacterial count after contacting with experimental samples (TNTs/ZnO-1, TNTs/ZnO-1 and TNTs/ZnO-3), and *A* represents the TNTs group.

2.2.2. Bacterial morphology. The bacterial morphology on all samples was observed by SEM (FEI, Nava450) after 24 h culturing. 2.5% glutaraldehyde was used to fix the bacteria on the surface for 2 h at 4 °C before dehydration. The dehydration was according to graded concentrations of ethanol (30%, 50%, 60%, 70%, 80%, 90%, 95% and 100%), and finally dried with CO₂ prior to observation. All samples were sputter-coated with Au.

2.3. Macrophage cell culture

Macrophage-like RAW 264.7 cells (murine leukemic monocyte cell line) purchased from China Infrastructure of Cell Line Resources were used in this work. The cell growth medium used to culture containing 10% fetal bovine serum (Gibco) and 1% penicillin/streptomycin (Invitrogen) in Dulbecco's Minimal Essential Medium (Hyclone). The cells were seeded at a density of 1 × 10⁴ cells cm⁻² in 24-well tissue culture plates (TCPs). Prior to macrophage seeding, all the samples were sterilized by soaking in 75% ethanol overnight, and washed three times for 30 min in distilled water, then exposed to ultraviolet light for 30 min.

2.3.1. Observation of the cell morphology. The morphology of macrophages adhering to the samples were observed by SEM. The cells were fixed with 2.5% glutaraldehyde for 2 h at room temperature. Before critical point dried with CO₂, all the samples were dehydrated through graded concentrations of ethanol (30%, 50%, 60%, 70%, 80%, 90%, 95% and 100%). The cells morphology were observed with a field-emission SEM (Zeiss, Germany) after being sputter-coated with a layer of Au.

2.3.2. Cell proliferation assays. Cell Counting Kit-8 (CCK-8, Dojin, Japan) was used to quantify the cell proliferation behavior. Briefly, after 2, 4 and 6 d of culture, the growth medium was removed and CCK-8 work solution (10% CCK-8 solution in serum free culture medium) was added into the plate for 1 h at 37 °C. Afterward, the absorbance was measured at a wavelength of 450 nm and recorded using a multi-mode plate reader (EnSpire, PerkinElmer). The cells cultured on TCP as the blank group.

2.3.3. Cell live/dead stain. The cellular viability cultured on the samples was identified through live/dead stain according to the manufacturer's instructions. After 2 d of culture, samples were stained with a calcein acetoxymethyl ester (calcein AM): propidium iodide (PI) solution (2 M: 10 μM, Dojin, Japan) for 10 min in the dark at room temperature. Then, the stain were terminated by washing the samples with PBS. Subsequently, the samples were visualized by an inverted fluorescence microscope (Zeiss, Germany).

2.4. Statistical analysis

All experiments were carried out in triplicate. Data are presented as the mean ± standard deviation. Statistical comparison

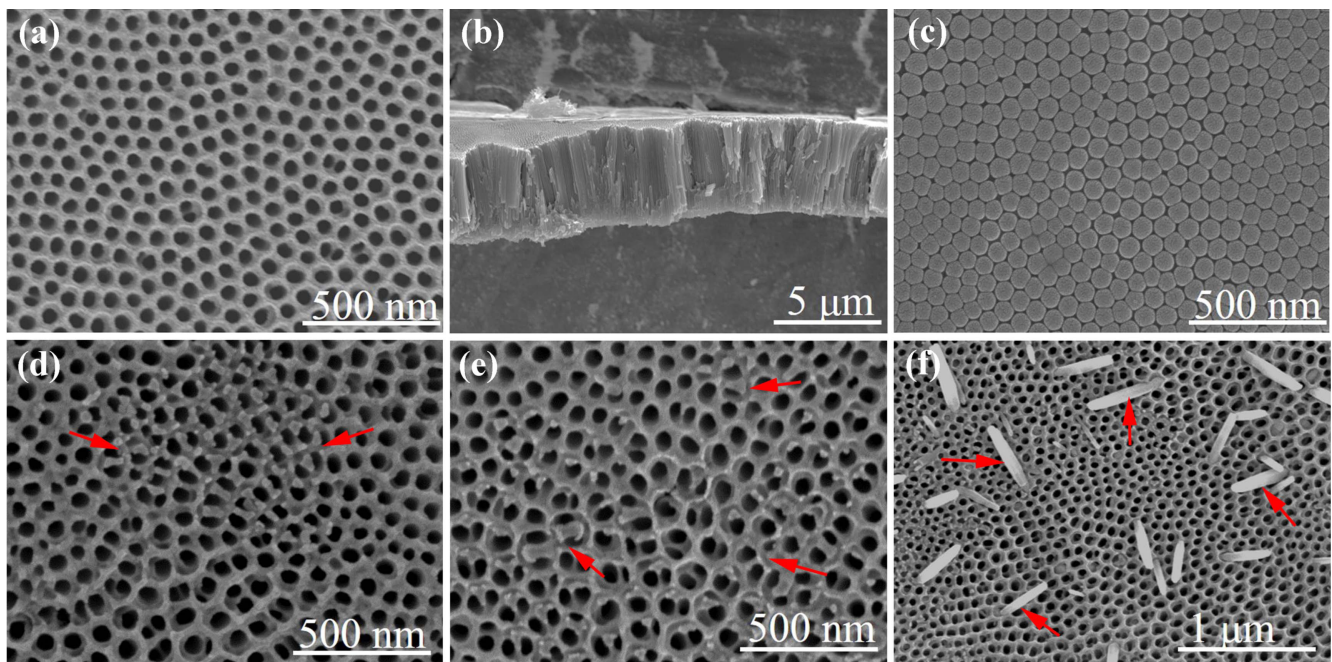


Figure 1. SEM images of the samples: (a) surface morphology of TNTs; (b) cross-section of TNTs; (c) bottom view of TNTs; surface morphology of: (d) TNTs/ZnO-1, (e) TNTs/ZnO-2 and (f) TNTs/ZnO-3.

was performed using ANOVA, and p -values < 0.05 are statistically significant.

3. Results and discussion

3.1. Characterization of TNTs/ZnO

As shown in figures 1(a)–(c), the TNTs with a length of $\sim 4 \mu\text{m}$ and $\sim 50 \text{ nm}$ inner diameter were prepared on the pure Ti surface. By varying electrolyte bath solution and reaction time, ZnO particles with different morphology and amount were deposited onto the TNTs. Irregular ZnO particles were observed on both of the TNTs/ZnO-1 and TNTs/ZnO-2 samples (figures 1(d) and (e)), and the particles density on the TNTs/ZnO-2 surface was higher and more homogeneous than TNTs/ZnO-1 surface. Nanorod ZnO particles were obtained by increasing the reaction time in low concentration of $\text{Zn}(\text{NO}_3)_2$ aqueous solution (figure 1(f)).

To further observe the distribution of the ZnO nanoparticles in the TNTs, TEM was used to identify the ZnO nanoparticles. With the incorporation of ZnO nanoparticles into the TNTs, a large amount of irregular nanoparticles was presented in the inner wall and the surface of the TNTs (figures 2(a) and (b)). Titania nanotubes were straight and the wall was smooth, as shown in figure 2(d). EDS analysis indicated that both Zn and O elements were observed in selected area (as shown in the red square frame), demonstrating the existence of irregular ZnO nanoparticles in the nanotubular cavities (figure 2(c)). The amount of deposited ZnO nanoparticles in the TNTs is listed in table 1. The average atomic percentage of Zn element was 2.09, 2.46 and

5.54 in TNTs/ZnO-1, TNTs/ZnO-2 and TNTs/ZnO-3 samples, respectively. The total Zn content that was measured by ICP showed that the concentration of Zn was 1.7 ppm and 3.4 ppm in TNTs/ZnO-1 and TNTs/ZnO-2, and reached 5.8 ppm in TNTs/ZnO-3 (table 1).

XPS was applied to detect the elements distribution. The XPS results revealed the presence of Ti, O, and Zn in all TNTs/ZnO samples (figure 3(a)). In the XPS spectra of Zn 2p from TNTs/ZnO (figure 3(b)), the Zn 2p_{1/2} peak position is located at 1044.8 eV and the binding energy of the Zn 2p_{3/2} peak position is 1021.7 eV, which fits with the Zn ion in ZnO. The XPS results also demonstrated the presence of ZnO in all groups of the TNTs/ZnO surface.

Compared with conventional metal implants, materials with nano-topographical surface coupled with a favorable surface chemistry, promoted adsorption of selective proteins such as vitronectin and fibronectin, and enhanced new bone formation. TNTs prepared by electrochemical anodization showed excellent biocompatibility, and their nanotubular structure was similar to the natural bone, which also improved the surface osteogenesis. However, the nanotubular topography on the surface also increased the bacterial adhesion and proliferation that may cause bacterial infection and implant failure. Thus, the nanotubular surface should be modified for the inhibiting or reducing bacterial attachment. Nanoparticles with antibacterial element incorporation into the TNTs was an effective and enduring method to improve the antibacterial properties compared with the antibiotic-loaded biodegradable polymers incorporation. Therefore, ZnO nanoparticles, which contained Zn ions, could reduce bacteria survival, and were incorporated into the TNTs to research the antibacterial activity.

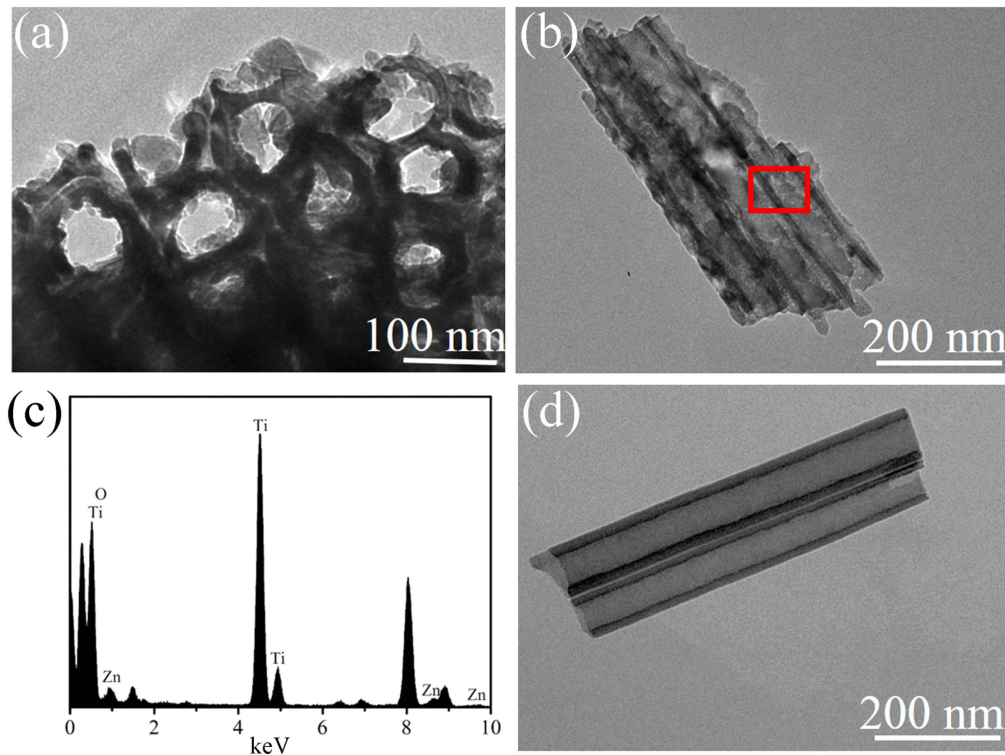


Figure 2. TEM images of: (a) top view and (b) cross-sectional view of the TNTs/ZnO-1; (c) EDS spectra of TNTs/ZnO-1 showing excited Zn on TNTs; (d) comparison of TNTs cross-sections.

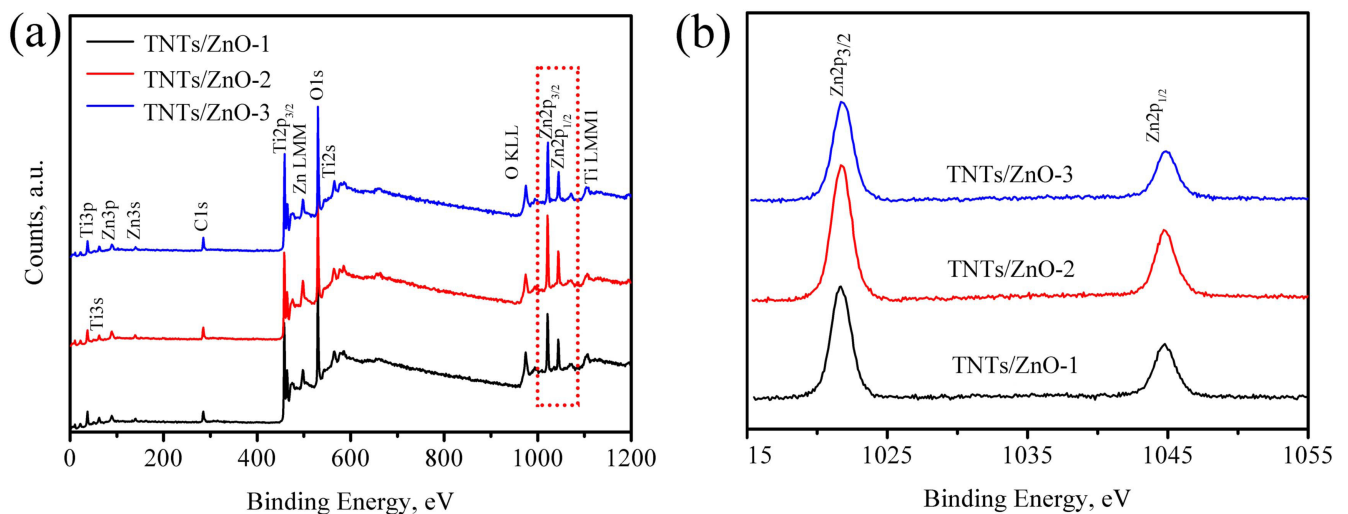


Figure 3. XPS spectra of elements in the samples: (a) the overall spectra; (b) XPS spectra of Zn2p with samples of ZnO-incorporated TNTs.

3.2. Zn ion release

It is well accepted that regulation of bacteria and cell behavior with ZnO nanoparticles highly relied on the release of Zn ions [37]. Nevertheless, the amount of Zn ions has to be strictly controlled to avoid cytotoxicity to the surrounding tissue. In this work, the released Zn ion concentration was measured by ICP-AES, shown in figures 4(a) and (b). During the immersion in PBS for 14 d, all the cumulative profiles show similar release characteristics, i.e. a burst release followed by a low level continuous release. The measured Zn ion concentration released from TNTs/ZnO-2 is greater than from TNTs/ZnO-

1 at each time point. Meanwhile, it was also found that the released concentration of Zn ions from TNTs/ZnO-3 was similar to TNTs/ZnO-2. These results demonstrated that the Zn ions release behavior was controlled by both Zn content and ZnO morphology. For the ZnO nanoparticles with irregular morphology, the release concentration highly depended on the Zn content. With the morphology change from irregular nanoparticles to nanorods, Zn ions release rate decreased. Thus, the morphology also affects the release behavior of Zn ions from the ZnO particles. In figure 4(b), the accumulated amount of Zn ions steadily increased during

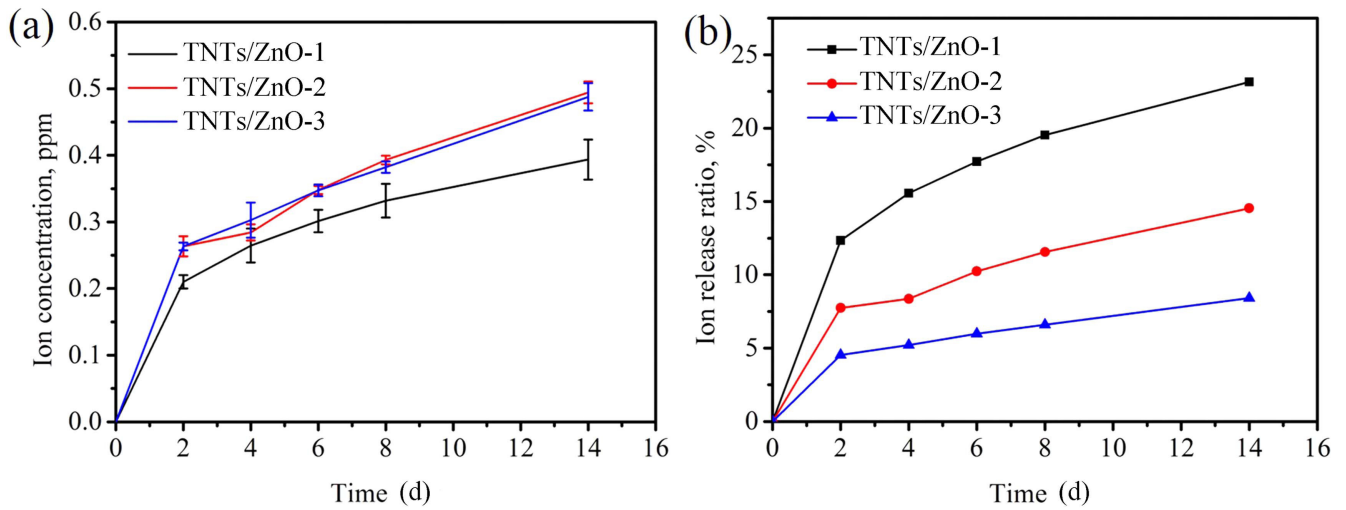


Figure 4. Zn ions concentration with respect to the immersion time. (a) The cumulative concentrations and (b) the average cumulative ion release ratio.

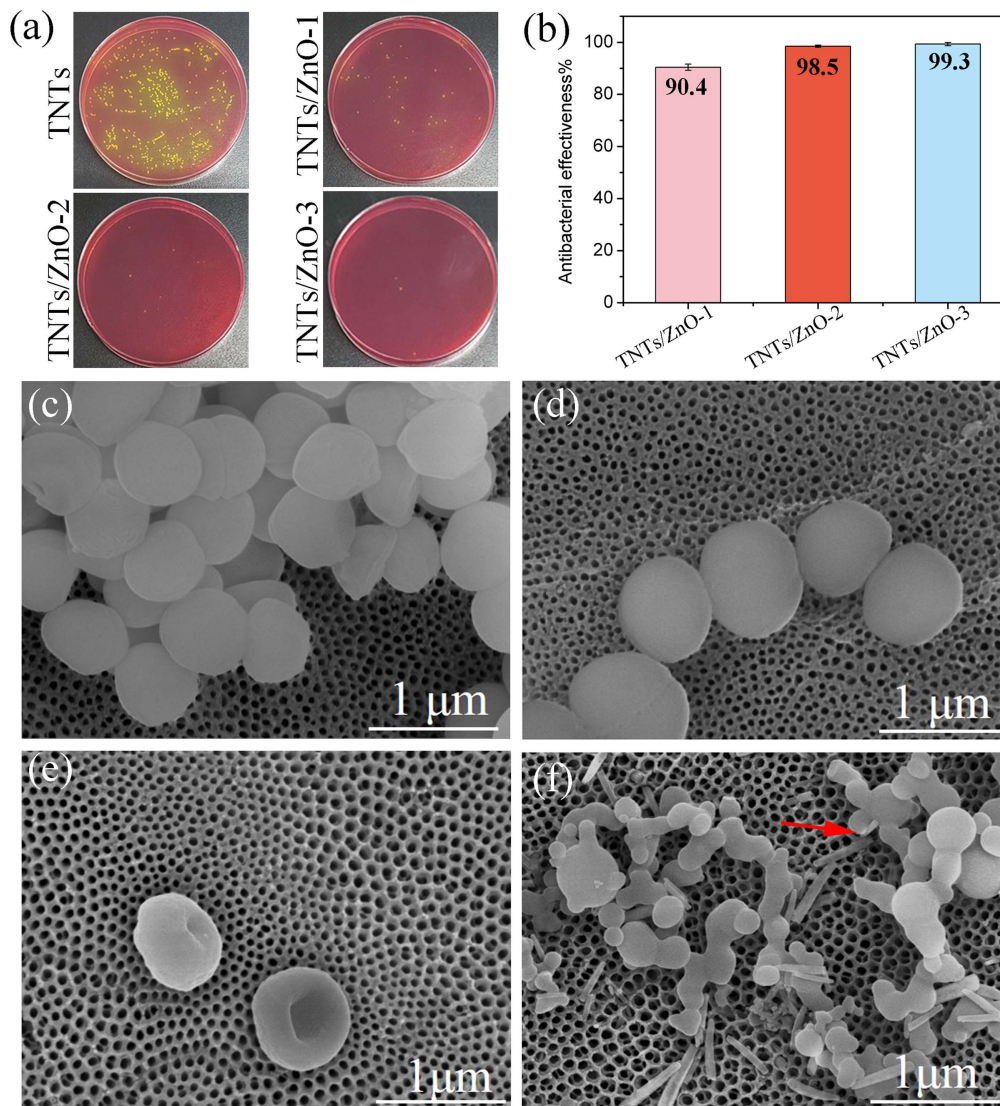


Figure 5. Short term bacteria incubation on the surface of TNTs/ZnO. (a) Typical image of *S. aureus* colonies from the samples after 1 d incubation; (b) the antibacterial effectiveness of TNTs/ZnO; SEM images of bacteria on: (c) TNTs, (d) TNTs/ZnO-1, (e) TNTs/ZnO-2 and (f) TNTs/ZnO-3.

the first 14 d. As expected, the amount of released Zn ions diminished with time.

3.3. Antibacterial activity

Bacterial infections highly affect the success of orthodontic/orthopedic implants [38]. Thus, it is expected that implant has the capability for the inhibition of bacterial adhesion and biofilm formation. ZnO nanoparticles, as one of the antibacterial agents on Ti-based implants, were proven to have an inhibitory effect on several kinds of Gram-positive and Gram-negative bacteria [33].

3.3.1. Contact-killing antibacterial activity. After 24 h culturing, the adhered bacteria survival on the samples were collected for the bacterial colony count experiment, as shown in figure 5(a). Compared with the TNTs group, all TNTs surfaces with ZnO nanoparticles could statistically and significantly kill the majority of bacteria, showing satisfactory antibacterial ability. The antibacterial effectiveness for different groups is summarized in figure 5(b). With the TNTs surface as the control group, average antibacterial effectiveness of all the ZnO samples was over 90% and the highest value reached 99.3%, showing excellent antibacterial ability. The SEM results (figures 5(c)–(f)) also demonstrated that the ZnO incorporated samples could significantly reduce the bacteria adhesion. As shown by the SEM images, the cell density on TNTs was the highest, which was in line with the colony count experiment. On the TNTs surface, the membrane of the bacteria was smooth and the shape of cells was spherical (figure 5(c)). With the incorporation of ZnO nanoparticles into the TNTs, the cell density decreased and the cell morphology became deformed. Especially on the TNTs surface with nanorod ZnO particles, the membrane of the cells was damaged, causing intracellular material efflux, shown with an arrow in figure 5(f). Therefore, not only the released Zn ions could inhibit the activity of bacteria, but also the morphology of the ZnO particles could affect the bacterial behavior.

3.3.2. Zn ion release antibacterial activity. The released Zn ion not only decided the amount of bacteria on the samples surface, but also affected the morphology of the bacteria. *S. aureus*, a typical gram-positive bacteria, showed low activity once exposed to the ZnO environment. That may be because of Zn ion that was released from ZnO nanoparticles reacted with the plasma membrane, and even some Zn ion entered into the cells to damage the intracellular balance of ions and lead to bacteria death. Moreover, Zn ion could be freed from the death bacteria and then act on others, which led to a long-term antibacterial process. The TNTs incorporated with ZnO showed excellent antibacterial properties, which were improved with the increasing ZnO content. The TNTs/ZnO-3 showed similar Zn ion release profile with the TNTs/ZnO-2, and showed better bactericidal performance that may be due to the nanorod shape easier penetrated into the bacterial membranes compared with the irregular nanoparticles. Thus, the morphology of the nanoparticles

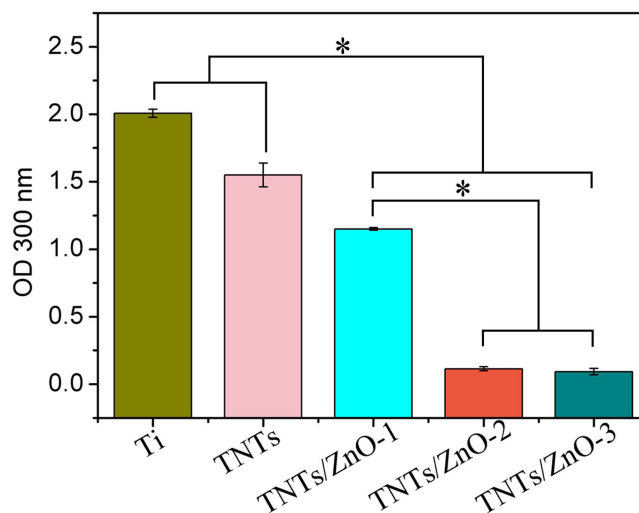


Figure 6. The bacteria density in supernatant after 24 h culture. Error bars represent standard deviation for three specimens for each piece of data. *Statistical significance ($p < 0.05$).

could have an additional effect with the Zn ions in antibacterial activity.

To further evaluate the released Zn ion antibacterial activity, the density of *S. aureus* in the supernatant was detected by ultraviolet spectrophotometer at a wavelength of 300 nm. Results are presented in figure 6. All TNTs with ZnO nanoparticles showed significantly low bacteria density in the supernatant compared with both polished Ti and TNTs. Zn ions released into the culture medium could obviously reduce the amount of surviving bacteria. Both surviving bacteria density on TNTs/ZnO-2 and TNTs/ZnO-3 had similar Zn ions release profiles, significantly lower than the TNTs/ZnO-1 group, which proved that the released Zn ions concentration decided the survival of bacteria in the supernatant.

3.4. Macrophage cells assay

Macrophages, a class of myeloid leukocytes with phagocytic activity and inflammatory signaling properties, play a pivotal role in antibacterial defense and tissue homeostasis. However, uncontrolled cytokines and inflammatory mediators may lead to excessive, even self-destructive cellular responses, which can be detrimental to dental/orthopedic implants [39]. After 2, 4 and 6 d, the macrophages proliferation was evaluated by the CCK-8. As shown in figure 7, the number of cells did not significantly increase at 4 and 6 d, which demonstrated that the samples with ZnO nanoparticles could inhibit the proliferation of macrophages RAW 264.7. The number of cells on TNTs/ZnO-2 and TNTs/ZnO-3 was significantly lower than the TNTs/ZnO-1 group at each time point, which proved that the higher ZnO content may cause cell apoptosis.

To confirm the macrophage cell status, live/dead stain and SEM were used after 2 d culture, and the results are shown in figure 8. In the fluorescence images in figures 8((a), (c), (e) and (g)), live cells were labeled green because the non-fluorescent calcein AM was converted to green-fluorescent calcein in live cells, while dead cells were red due to DNA binding of ethidium homodimer in cells with compromised

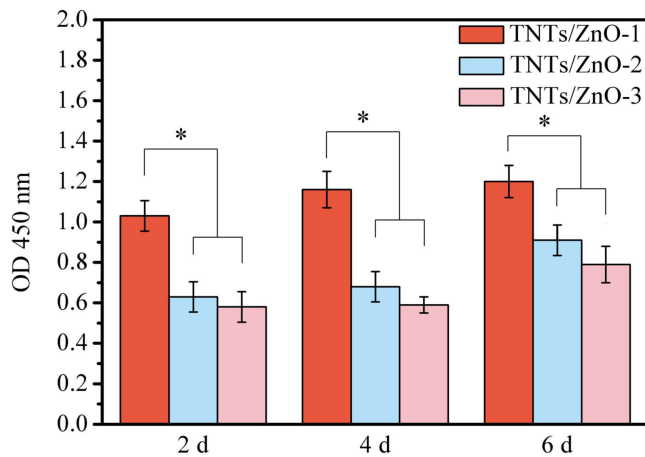


Figure 7. Macrophage cells proliferation on various sample surfaces evaluated by the CCK-8 assay. Error bars represent standard deviation for three specimens for each piece of data. *Statistical significance ($p < 0.05$).

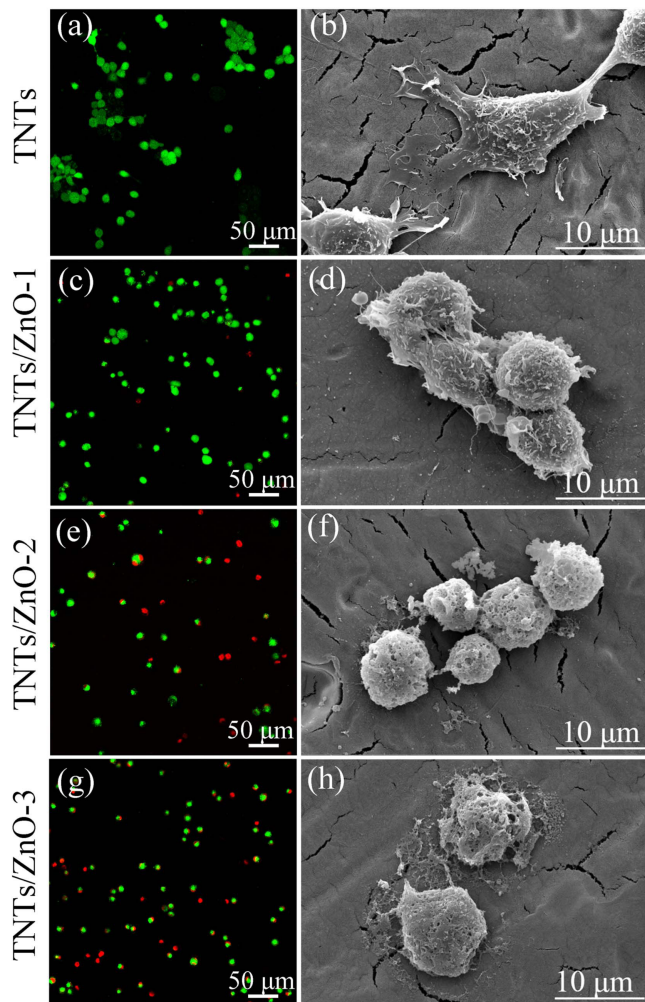


Figure 8. Fluorescence images showing the live/dead assays: (a) TNTs, (c) TNTs/ZnO-1, (e) TNTs/ZnO-2 and (g) TNTs/ZnO-3; the morphology of cell adherent at 2 d post-seeding: (b) TNTs, (d) TNTs/ZnO-1, (f) TNTs/ZnO-2 and (h) TNTs/ZnO-3. Green = live cells; red = dead cells.

nuclear membranes. Although the cell density was similar in all groups, the number of dead cells increased with the amount of incorporated ZnO. Especially for the high dose of ZnO groups (TNTs/ZnO-2 and TNTs/ZnO-3), there was a large amount of dead cells labeled with red color, which was consistent with the CCK-8 results. After 2 d culturing, SEM was used to observe the morphology and adherence of macrophage cells. As shown in figure 8(b), the cells on the surface of TNTs had polygonal morphology and spread well, and elongated pseudopodia on the edge of cells were observed. For the TNTs/ZnO-1 surface, the adherent area of macrophages reduced and no obvious pseudopodium was observed. Moreover, with the increased dose of ZnO (TNTs/ZnO-2 and TNTs/ZnO-3), the membrane of the cells was damaged and penetrated. Comparing to the irregular nanoparticles, the macrophages did not show more sensitive to the nanorods structure. The morphology of macrophages mainly depends on the Zn ion concentration in the culture medium.

Compared to TNTs, the results of the CCK-8 and the live/dead stain showed that there were fewer macrophage cells on the TNTs/ZnO surface, and all cells were in lower activity and proliferation, which demonstrated that ZnO reduced the activity of macrophages in high concentration. Moreover, the macrophages curled up into spherical shape, which reduced the macrophages adhesion and extension, leading to macrophages dysplasia and low levels of inflammatory cytokines secretion [40]. A similar result was noted by Pati *et al* [39], who found dose-dependent decrease in the number of live cells, along with inhibited macrophages migration at higher ZnO nanoparticles concentration. Additionally, ZnO nanoparticles in high concentration would lead to cytotoxicity, such as the rat mesenchymal stem cells (rMSCs) remained 50% viable when the concentration of Zn ions was over 10 ppm [33, 34] and human osteogenic sarcoma (U-2OS) retained 50% viability at 11.7 ppm [41]. In our work, the daily Zn ion release amount of all TNTs/ZnO samples was lower than the reported, which could inhibit the viability of macrophages with low cytotoxicity to other cells.

4. Conclusions

In this work, ZnO nanoparticles were incorporated into TiO₂ nanotubes by the electro-deposition method. The TNTs/ZnO samples could inhibit the proliferation and viability of *S. aureus* through the release Zn ions and nanoscale structure. Compared with the irregular ZnO nanoparticles, the nanorod ZnO particles on the TNTs surface showed easier penetration into bacteria membrane, and improved the antibacterial properties. Moreover, the RAW 264.7 cultured on the TNTs/ZnO samples displayed poor activity and all cells were curled up to be spherical shape without pseudopodia extension, which decreased the immune response. In summary, TNTs/ZnO in the present work showed excellent antibacterial properties and positive behavior to weaken immune response. Further experiment will be continued

to optimize the promising properties and achieved lower cytotoxicity for wide applications in the future implantation field.

Acknowledgments

This work was supported by the National Natural Science Foundation of China (Grant Nos. 51501008 and U1560103), China Postdoctoral Science Foundation (2016M591075) and Fundamental Research Funds for the Central Universities (2302016FRF-TP-16-001A1).

ORCID iDs

Shenglian Yao  <https://orcid.org/0000-0001-7734-9399>

Yudong Zheng  <https://orcid.org/0000-0002-4218-5280>

References

- [1] Minagar S, Berndt C C, Wang J, Ivanova E and Wen C 2012 A review of the application of anodization for the fabrication of nanotubes on metal implant surfaces *Acta Biomater.* **8** 2875–88
- [2] Roy P, Berger S and Schmuki P 2011 TiO₂ nanotubes: synthesis and applications *Angew. Chem. Int. Ed. Engl.* **50** 2904–39
- [3] Brammer K S, Frandsen C J and Jin S 2012 TiO₂ nanotubes for bone regeneration *Trends Biotechnol.* **30** 315–22
- [4] Fan R and Wan J 2017 Electrode distance regulates the anodic growth of titanium dioxide (TiO₂) nanotubes *Nanotechnology* **28** 25LT01
- [5] Zhao L, Liu L, Wu Z, Zhang Y and Chu P K 2012 Effects of micropitted/nanotubular titania topographies on bone mesenchymal stem cell osteogenic differentiation *Biomaterials* **33** 2629–41
- [6] Brammer K S, Oh S, Gallagher J O and Jin S 2009 Enhanced cellular mobility guided by TiO₂ nanotube surfaces *Nano Lett.* **8** 786–93
- [7] Ma Q L, Zhao L Z, Liu R R, Jin B Q, Song W, Wang Y, Zhang Y S, Chen L H and Zhang Y M 2014 Improved implant osseointegration of a nanostructured titanium surface via mediation of macrophage polarization *Biomaterials* **35** 9853–67
- [8] Lavenus S, Berreur M, Trichet V, Pilet P, Louarn G and Layrolle P 2011 Adhesion and osteogenic differentiation of human mesenchymal stem cells on titanium nanopores *Eur. Cell. Mater.* **22** 84–96
- [9] Elizabeth E, Baranwal G, Krishnan A G, Denon D and Nair M 2014 ZnO nanoparticle incorporated nanostructured metallic titanium for increased mesenchymal stem cell response and antibacterial activity *Nanotechnology* **25** 337–45
- [10] Khurana C, Sharma P, Pandey O P and Chudasama B 2016 Synergistic effect of metal nanoparticles on the antimicrobial activities of antibiotics against biorecycling microbes *J. Mater. Sci. Technol.* **32** 524–32
- [11] Jin S, Ren L and Yang K 2016 Bio-functional Cu containing biomaterials: a new way to enhance bio-adaption of biomaterials *J. Mater. Sci. Technol.* **32** 835–9
- [12] Alswat A A, Ahmad M B, Hussein M Z, Ibrahim N A and Saleh T A 2017 Copper oxide nanoparticles-loaded zeolite and its characteristics and antibacterial activities *J. Mater. Sci. Technol.* **33** 889–96
- [13] Popat K C, Eltgroth M, Latempa T J, Grimes C A and Desai T A 2007 Decreased *Staphylococcus epidermis* adhesion and increased osteoblast functionality on antibiotic-loaded titania nanotubes *Biomaterials* **28** 4880–8
- [14] Zhang H, Sun Y, Tian A, Xue X X, Wang L, Alquhali A and Bai X 2013 Improved antibacterial activity and biocompatibility on vancomycin-loaded TiO₂ nanotubes: *in vivo* and *in vitro* studies *Int. J. Nanomed.* **8** 4379–89
- [15] Yao C and Webster T J 2009 Prolonged antibiotic delivery from anodized nanotubular titanium using a co-precipitation drug loading method *J. Biomed. Mater. Res. Appl. Biomater. B* **91** 587–95
- [16] Ma M, Kazemzadeh Narbat M, Hui Y, Lu S, Ding C, Chen D D, Hancock R E and Wang R 2012 Local delivery of antibacterial peptides using self-organized TiO₂ nanotube arrays for peri-implant infections *J. Biomed. Mater. Res. A* **100** 278–85
- [17] Zhao L, Wang H, Huo K, Cui L, Zhang W, Ni H, Zhang Y, Wu Z and Chu P K 2011 Antibacterial nano-structured titania coating incorporated with silver nanoparticles *Biomaterials* **32** 5706–16
- [18] Roguska A, Belcarz A, Pisarek M, Ginalska G and Lewandowska M 2015 TiO₂ nanotube composite layers as delivery system for ZnO and Ag nanoparticles—an unexpected overdose effect decreasing their antibacterial efficacy *Mater. Sci. Eng. C* **51** 158–66
- [19] Li J, Sang H, Guo H, Popko J T, He L, White J C, Parkash Dhankher O, Jung G and Xing B 2017 Antifungal mechanisms of ZnO and Ag nanoparticles to sclerotinia homeocarpa *Nanotechnology* **28** 155101
- [20] Khan S T, Ahmad J, Ahamed M, Musarrat J and Alkhedhairy A A 2016 Zinc oxide and titanium dioxide nanoparticles induce oxidative stress, inhibit growth, and attenuate biofilm formation activity of streptococcus mitis *J. Biol. Inorg. Chem.* **21** 295–303
- [21] Aponiene K, Serevičius T, Luksiene Z and Jursenas S 2017 Inactivation of bacterial biofilms by visible light-activated unmodified ZnO nanorods *Nanotechnology* **28** 365701
- [22] Dong Y, Yan Y, Ma H, Zhang S, Li J, Xia C, Shi S Q and Cai L 2016 *In situ* chemosynthesis of ZnO nanoparticles to endow wood with antibacterial and UV-resistance properties *J. Mater. Sci. Technol.* **33** 266–70
- [23] Liu W, Golshan N H, Deng X, Hickey D J, Zeimer K, Li H and Webster T J 2016 Selenium nanoparticles incorporated into titania nanotubes inhibit bacterial growth and macrophage proliferation *Nanoscale* **8** 15783–94
- [24] Tran P A, O'Brien-Simpson N, Reynolds E C, Pantarat N, Biswas D P and O'Connor A J 2016 Low cytotoxic trace element selenium nanoparticles and their differential antimicrobial properties against *S. aureus* and *E. coli* *Nanotechnology* **27** 45101–10
- [25] Roguska A, Belcarz A, Pisarek M, Ginalska G and Lewandowska M 2015 TiO₂ nanotube composite layers as delivery system for ZnO and Ag nanoparticles—an unexpected overdose effect decreasing their antibacterial efficacy *Mater. Sci. Eng. C* **51** 158–66
- [26] Parkin J and Cohen B 2001 An overview of the immune system *Lancet* **357** 1777–89
- [27] Scislowska Czarnecka A, Menaszek E, Szaraniec B and Kolaczowska E 2012 Ceramic modifications of porous titanium: effects on macrophage activation *Tissue Cell* **44** 391–400
- [28] Lü W L, Wang N, Gao P, Li C Y, Zhao H S and Zhang Z T 2015 Effects of anodic titanium dioxide nanotubes of different diameters on macrophage secretion and expression of cytokines and chemokines *Cell Proliferation* **48** 95–104
- [29] Song W, Zhang J, Guo J, Zhang J, Ding F, Li L and Sun Z 2010 Role of the dissolved zinc ion and reactive oxygen species in cytotoxicity of ZnO nanoparticles *Toxicol. Lett.* **199** 389–97

- [30] Neacsu P, Mazare A, Cimpean A, Park J, Costache M, Schmuki P and Demetrescu I 2014 Reduced inflammatory activity of RAW 264.7 macrophages on titania nanotube modified Ti surface *Int. J. Biochem. Cell Biol.* **55** 187–95
- [31] Giovanni M, Yue J, Zhang L, Xie J, Ong C N and Leong D T 2015 Pro-inflammatory responses of RAW264.7 macrophages when treated with ultralow concentrations of silver, titanium dioxide, and zinc oxide nanoparticles *J. Hazard Mater.* **297** 146–52
- [32] Applerot G, Lipovsky A, Dror R, Perkas N, Nitzan Y, Lubart R and Gedanken A 2009 Enhanced antibacterial activity of nanocrystalline ZnO due to increased ROS-mediated cell injury *Adv. Funct. Mater.* **19** 842–52
- [33] Liu W, Su P, Chen S, Wang N, Ma Y, Liu Y, Wang J, Zhang Z, Li H and Webster T J 2014 Synthesis of TiO₂ nanotubes with ZnO nanoparticles to achieve antibacterial properties and stem cell compatibility *Nanoscale* **6** 9050–62
- [34] Liu W, Su P, Gonzales A, Chen S, Wang N, Wang J, Li H, Zhang Z and Webster T J 2015 Optimizing stem cell functions and antibacterial properties of TiO₂ nanotubes incorporated with ZnO nanoparticles: experiments and modeling *Int. J. Nanomed.* **10** 1997–2019
- [35] Yao S, Feng X, Li W, Wang L N and Wang X 2017 Regulation of RAW 264.7 macrophages behavior on anodic TiO₂ nanotubular arrays *Frontiers Mater. Sci.* **1** 1–10
- [36] Jiang S, Wu Q, Zhou Y, Wen Y, Yang C and Zhang S 2007 Effects of electrodeposition conditions on the microstructures of ZnO thin films *Integr. Ferroelectr.* **88** 33–43
- [37] Chang Y N, Zhang M, Xia L, Zhang J and Xing G 2012 The toxic effects and mechanisms of CuO and ZnO nanoparticles *Materials* **5** 2850–71
- [38] Zilberman M and Elsner J J 2008 Antibiotic-eluting medical devices for various applications *J. Control. Release* **130** 202–15
- [39] Pati R, Das I, Mehta R K, Sahu R and Sonawane A 2016 Zinc-oxide nanoparticles exhibit genotoxic, clastogenic, cytotoxic and actin depolymerization effects by inducing oxidative stress responses in macrophages and adult mice *Toxicol. Sci.* **150** 454–72
- [40] Khandwekar A and Rho C K 2012 Modulation of cellular responses on engineered polyurethane implants *J. Biomed. Mater. Res. A* **100** 2211–22
- [41] Kubásek J, Vojtěch D, Jablonská E, Pospisilová I, Lipov J and Ruml T 2016 Structure, mechanical characteristics and *in vitro* degradation, cytotoxicity, genotoxicity and mutagenicity of novel biodegradable Zn–Mg alloys *Mater. Sci. Eng. Mater. Biol. Appl. C* **58** 24–35